Retrospective retrieval of long-term consistent global leaf area index (1981–2011) from combined AVHRR and MODIS data

Yang Liu,[1] Ronggao Liu,[1] and Jing M. Chen[2,3]

Received 25 May 2012; revised 4 September 2012; accepted 8 September 2012; published 18 October 2012.

[1] In this paper, we present an approach for generating a consistent long-term global leaf area index (LAI) product (1981–2011) by quantitative fusion of Moderate Resolution Imaging Spectroradiometer (MODIS) and historical Advanced Very High Resolution Radiometer (AVHRR) data. First, a MODIS LAI series was generated from MODIS data based on the GLOBCARBON LAI algorithm. Then, the relationships between AVHRR observations and MODIS LAI were established pixel by pixel using two data series during overlapped period (2000–2006). Then the AVHRR LAI back to 1981 was estimated from historical AVHRR observations based on these pixel-level relationships. The long-term LAI series was made up by combination of AVHRR LAI (1981–2000) and MODIS LAI (2000–2011). The LAI derived from AVHRR was intercompared with that from MODIS during the overlapped period. The results show that the LAIs from these two different sensors are good consistency, with LAI differences are within ±0.6 over 99.0% vegetated pixels. The long-term LAI was also compared with field measurements, which has an error of 0.81 LAI on average. Compared with the LAI retrieved directly from the GLOBCARBON algorithm, the LAI derived by our method has a lower temporal noise, which means uncertainties from the low quality of AVHRR measurements can be reduced with the aid of high-quality MODIS data. This product is hosted on the GlobalMapping Web site (http://www.globalmapping.org/globalLAI) for free download, which will provide a long-term LAI over 30 years for modeling the carbon and water cycles.

Citation: Liu, Y., R. Liu, and J. M. Chen (2012), Retrospective retrieval of long-term consistent global leaf area index (1981–2011) from combined AVHRR and MODIS data, *J. Geophys. Res.*, *117*, G04003, doi:10.1029/2012JG002084.

1. Introduction

[2] The world is experiencing persistent climate warming, which will alter the vegetation structure, and the vegetation feedback to the climate might amplify or dampen regional and global climate change [*Ciais et al.*, 2005; *Heimann and Reichstein*, 2008]. The leaf area index (LAI), which is commonly defined as half the total all-sided developed area of green leaves per unit ground surface area [*Chen and Black*, 1992], is a critical parameter for modeling vegetation's water, carbon, and energy exchange with the atmosphere [*Braswell et al.*, 1997; *Gitelson and Kaufman*, 1998]. To better understand the interaction of terrestrial vegetation and the climate, the global long-term LAI should be quantified [*Global Climate Observing System*, 2006].

[3] Various sensors onboard satellite platforms have taken global snapshots since the 1970s, such as NOAA/AVHRR, SPOT/VEGETATION, TERRA-AQUA/MODIS, ENVISAT/MERIS, and TERRA/MISR. Several global and regional LAI products from those different sensors have been provided routinely, such as ECOCLIMAP [*Masson et al.*, 2003] and ISLSCP-II (1982–1990) [*Los et al.*, 2000] from AVHRR, CYCLOPES (1999–2007) [*Baret et al.*, 2007], GLOBCARBON (1998–2003) [*Deng et al.*, 2006] and Canada-wide LAI map (1993–2002) [*Chen et al.*, 2002] from VEGETATION, MERIS LAI (2002–) [*Bacour et al.*, 2006], MOD15 (2000–) from MODIS [*Myneni et al.*, 2002], and MISR LAI (2000–) [*Diner et al.*, 2008]. Some of these products have been applied to study the global carbon and water cycles [e.g., *Zhao and Running*, 2010; *Leuning et al.*, 2008]. However, these products, which are all generated from single sensor observations, are limited in their temporal coverage. Also, due to the discrepancies of sensors characteristics and retrieval algorithms, these various LAI products are not consistent enough to be directly combined to make up a long-term LAI series. To retrospectively estimate evapotranspiration [*Zhang et al.*, 2010] or vegetation primary productivity [*Piao et al.*, 2009] back to the 1980s, the LAI-related vegetation parameters are inferred

[1]Institute of Geographic Sciences and Natural Resources Research, Chinese Academy of Sciences, Beijing, China.
[2]International Institute of Earth System Science, Nanjing University, Nanjing, China.
[3]Department of Geography, University of Toronto, Toronto, Ontario, Canada.

Corresponding author: R. Liu, Institute of Geographic Sciences and Natural Resources Research, Chinese Academy of Sciences, 11A Datun Rd., Beijing 100101, China. (liurg@igsnrr.ac.cn)

0148-0227/12/2012JG002084

directly from the long-term NDVI, which may introduce a large uncertainty because the relationship between NDVI and the vegetation parameter varies from site to site due to the diverse canopy and background conditions [*Baret and Guyot*, 1991]. Moreover, the NDVI is also not consistent among the different sensors [*Tarnavsky et al.*, 2008]. Therefore, it is valuable to design a new algorithm to seamlessly fuse the multisource data to produce a consistent long-term LAI series.

[4] The AVHRR sensors onboard the NOAA 7–14 satellite series have observed the earth continuously since 1981. Since 2000, the advanced sensor MODIS, onboard the Terra and Aqua satellites, has provided a more reliable data source for LAI estimation with its better spectral, temporal and spatial resolutions as well as georeference and calibration accuracy. The combination of observations from MODIS and AVHRR may be a feasible approach to deriving long-term LAI records back to 1981. However, the differences in data information content due to various sensor spectral characteristics, spatial and temporal resolutions, calibration and geometry make it challenging to do so. For example, the reflectance from AVHRR and MODIS are not consistent even in the same atmospheric and terrestrial state [*Gitelson and Kaufman*, 1998; *Trishchenko et al.*, 2002]. Some attempts have been made recently to take these differences into account to generate a long-term LAI data set (1981–2006) from AVHRR data with a comparable quality to MODIS MOD15 LAI by a physically based radiative transfer approach, with parameterization of canopy spectral bidirectional reflectance with consideration of the spectral bandwidth and spatial resolution differences among sensors [*Ganguly et al.*, 2008a]. However, the red and near-infrared channels of AVHRR are spectrally broad, which are highly sensitive to atmospheric conditions, while the atmospheric contamination on these bands are nearly impossible to correct without the SWIR bands. In addition, the reflective channels are only calibrated preflight and fewer bands available. These factors determine that the data quality of AVHRR should be lower than that of MODIS, which means the LAI directly derived from AVHRR by the traditional retrieval procedures should be inferior to that of MODIS.

[5] The vegetation index (VI), though which carries only a fraction of the information available in the original NIR/red bands, can enhance the information of vegetation while lessens the ill effects of other factors, such as canopy structural shadows, soil/background, angular anisotropy and atmospheric contamination, because of the correlation of the noise between the red/NIR bands [*Chen*, 1996]. And the VI correlates highly with the ground LAI measurements for various biomes, such as grassland, cropland and coniferous and deciduous forests [e.g., *Fava et al.*, 2009; *Aparicio et al.*, 2002; *Spanner et al.*, 1994; *Heiskanen*, 2006; *Kraus et al.*, 2009]. So, if the relationship between VI and LAI can be established, retrieval of LAI from the VI should be better than that directly from the band reflectances. Unfortunately, the VI-LAI relationship varies from site to site that make it impossible to establish this relationship using the measured field LAI and the VI from satellite data for a global scale. Since the MODIS are more advanced than AVHRR, it can be believed that if the LAI from MODIS was taken as a reference to establish the pixel-based VI-LAI relationship for AVHRR, the quality of LAI derived from AVHRR is more likely improved.

[6] The Simple Ratio (SR), the ratio of the near-infrared (NIR) to red band land surface reflectance, is nearly linearly related to LAI. In this paper, an approach based on the pixel-based SR-LAI relationships is presented to generate a long-term (1981–2011) global LAI product through the combination of MODIS and historical AVHRR data. The SR-LAI relationships are established pixel-by-pixel by the LAI derived from MODIS and the SR from AVHRR, and then the LAI from historical AVHRR observations are retrieved based on these relationships. Because these SR-LAI relationships are based on the MODIS LAI, the LAI derived from AVHRR should be consistent with MODIS LAI. The outline of this paper is as follows. A brief introduction of data sets is presented in section 2. The implementation of the algorithm is detailed in section 3. Section 4 presents the results of the algorithm and evaluates its performances. The limitation and potential improvements of the algorithm are discussed in section 5. Finally, the conclusion is presented in section 6.

2. Data

2.1. GIMMS NDVI and MODIS Data

[7] The Global Inventory Modeling and Mapping Studies (GIMMS) NDVI data set from AVHRR (1981–2006) and several MODIS products (2000–2011) are used in this study. The LAI for AVHRR and MODIS are retrieved from GIMMS NDVI and MODIS land surface reflectance product MOD09A1, respectively. The land cover type is defined by MODIS land cover product MCD12Q1. The performance of the algorithm is compared with the MODIS LAI product MOD15A2.

[8] GIMMS provides NDVI two times per month with a spatial resolution of 4/55 degrees (approximately 8 km) of the geographic coordinate over the global land surface except Greenland and Antarctica (63°S–90°N, 180°W–180°E) and spanning from July 1981 through December 2006. These data sets were derived from observations of the AVHRR instrument onboard the NOAA satellite series 7, 9, 11, 14, 16, and 17. The GIMMS NDVI has been corrected for residual sensor degradation and sensor intercalibration differences, view geometry effects due to satellite drift, distortions caused by persistent cloud cover globally, aerosols of the two major volcanic eruptions and other effects not related to vegetation change [*Tucker et al.*, 2005]. Flag files are also provided to indicate the quality of the corresponding NDVI values. The flag value ranges from 0 to 6, with a good flag value equal to 0 or 1. All of the GIMMS NDVI data were downloaded from http://glcf.umiacs.umd.edu/data/gimms/.

[9] The MODIS Surface Reflectance Product (MOD09) contains the surface reflectance in seven spectral bands. MOD09A1 provides global 8 day composite 500 m land surface reflectance with atmospheric effects corrected since February 2000. The MODIS land cover product (MCD12Q1) supplies a yearly 500 m land cover classification map of the globe derived through a supervised decision tree classification method with 5 different classification schemes. In this study, the IGBP global vegetation classification scheme product is selected, which includes 11 natural vegetation classes, three developed and mosaicked land classes and three nonvegetated land classes. The MODIS MOD15 LAI product contains a global 8 day composite true LAI of the land surface in a 1 × 1 km grid by the inversion of a three-dimensional radiative

Table 1. Summary of Fine Resolution LAI Maps Used for Validation With the GLOBMAP LAI

Site (Country)	Latitude	Longitude	Biome	Date	Mean LAI	CI	Reference
Baohe (China)	34.22	107.23	MF	early June 2003	3.8	Y	*Chen et al.* [2007]
Liping (China)	26.27	109.24	MF	15 Aug 2003	3.8	Y	*Zheng et al.* [2007]
Jian (China)	26.88	115.06	NF	24–27 Jul 2008	2.6	Y	*Li et al.* [2010]
Maoershan (China)	45.37	127.60	MF	12–18 Jul 2009	4.7	Y	*Zhu et al.* [2010]
Hulunbeier (China)	49.34	119.99	Grass	21–26 Jun 2010	1.5	Y	*Liu et al.* [2011]
Xilinhaote (China)	43.62	116.71	Grass	28 Jun 2010 to 3 Jul 2010	1.2	Y	*Liu et al.* [2011]
Chequamegon (USA)	45.95	−90.27	MF	1 Aug 2002	3.4	N	BigFoot[b]
Harvard (USA)	42.53	−72.17	MF	26 Jul 2001	4.6	N	BigFoot[b]
				24 Aug 2002	4.7	N	BigFoot[b]
Konza (USA)	39.09	−96.57	Grass	16 Aug 2001	2.6	Y	BigFoot[b]
				18 Jun 2001	2.9	Y	BigFoot[b]
Metolius (USA)	44.45	−121.57	NF	24 Sep 2002	2.5	N	BigFoot[b]
Sevilleta (USA)	34.35	−106.69	Grass	26 Jul 2002	0.1	Y	BigFoot[b]
				22 Aug 2002	0.3	Y	BigFoot[b]
				9 Sep 2002	0.4	Y	BigFoot[b]
				15 Nov 2002	0.3	Y	BigFoot[b]
				23 Jun 2003	0.6	Y	BigFoot[b]
				28 Jul 2003	0.5	Y	BigFoot[b]
				15 Sep 2003	0.5	Y	BigFoot[b]
				21 Nov 2003	1.0	Y	BigFoot[b]
Tapajos (Brazil)	−2.87	−54.95	EBF	15 Feb 2002	6.1	N	BigFoot[b]
Alpilles01 (France)	43.81	4.75	Crop	15 Mar 2001	1.0	N	*Yang et al.* [2006][b]
Flakaliden (Sweden)	64.11	19.47	NF	20 Aug 2002	2.3	N	*Yang et al.* [2006]
Ruokolahti (Finland)	61.53	28.71	NF	10 Jun 2000	1.7	Y	*Yang et al.* [2006][b]
Larose (Canada)	45.38	−75.17	MF	19 Aug 2003	3.2	Y	CCRS[a]
Appomattox (USA)	37.22	−78.88	MF	5 Aug 2002	1.9	Y	*Iiames et al.* [2004][b]
Los Inocentes (Costa Rica)	11.03	−85.5	EBF	15 Jun 2000	2.5	N	*Kalacska et al.* [2004][b]
AekLoba (Sumatra)	2.63	99.58	EBF	1 Jun 2001	3.5	N	*Garrigues et al.* [2008]
Alpilles02 (France)	43.81	4.71	Crop	20 Jul 2002	1.7	Y	*Garrigues et al.* [2008]
Barrax (Spain)	39.07	−2.10	Crop	3 Jul 2003	1.0	N	*Garrigues et al.* [2008]
Concepcion (Chile)	−37.47	−73.47	NF	23 Jan 2003	3.1	N	*Garrigues et al.* [2008]
Gilching (Germany)	48.08	11.32	Crop	8 Jul 2002	5.4	Y	*Garrigues et al.* [2008]
Gourma (Mali)	15.32	−1.56	Grass	1 Oct 2001	1.2	N	*Garrigues et al.* [2008]
Haouz (Morocco)	31.66	−7.60	Crop	25 Mar 2003	1.2	N	*Garrigues et al.* [2008]
Hirsikangas (Finland)	62.64	27.01	NF	2 Aug 2003	2.5	N	*Garrigues et al.* [2008]
Jarvselja (Estonia)	58.3	27.26	MF	13 Jul 2002	4.2	N	*Garrigues et al.* [2008]
				26 Jun 2003	4.2	N	*Garrigues et al.* [2008]
Laprida (Argentina)	−36.99	−60.55	Grass	13 Nov 2002	2.8	Y	*Garrigues et al.* [2008]
Larzac (France)	43.94	3.12	Grass	12 Jul 2002	0.8	Y	*Garrigues et al.* [2008]
Rovaniemi (Finland)	66.46	25.35	NF	23 Jul 2004	1.3	N	*Garrigues et al.* [2008]
Sud-Ouest (France)	43.51	1.24	Crop	20 Jul 2002	2.0	Y	*Garrigues et al.* [2008]
Sonian (Belgium)	50.77	4.41	MF	28 Jul 2004	5.6	Y	*Garrigues et al.* [2008]
Nezer (France)	44.57	−1.05	NF	21 Apr 2002	2.1	Y	*Garrigues et al.* [2008]
Camerons (Australia)	−32.6	116.25	EBF	6 Apr 2004	2.1	Y	*Garrigues et al.* [2008]
Puechabon (France)	43.72	3.65	MF	12 Jun 2001	2.8	Y	*Garrigues et al.* [2008]

[a]CI stands for clumping status. For Biome, MF, NF and EBF stand for mixed forest, needleleaf forest and evergreen broadleaf forest, respectively. For CI, the value Y(N) means the clumping have (have not) been taken into account in the LAI measurement. For BigFoot, see *Cohen et al.* [2006] and for CCRS, see *Abuelgasim et al.* [2006].
[b]Also refer to *Garrigues et al.* [2008].

transfer model using a look-up table approach for eight biomes [*Myneni et al.*, 2002]. The back-up algorithm based on the relationship between LAI and NDVI is employed when the main algorithm fails. The MOD09A1, MCD12Q1 and MOD15A2 products are all provided in the Sinusoidal grid. All the MODIS data were downloaded from https://lpdaac.usgs.gov/.

[10] All data were preprocessed to the same projection with GIMMS NDVI data set. MOD09A1 and MCD12Q1 images from 2000 to 2011 were transformed to the geographic projection at a 500 m × 500 m spatial resolution through the nearest neighbor interpolation, 1000 m × 1000 m for MOD15A2. The reprojected data were composed to form global maps. The MODIS land surface reflectance and LAI standard products were then screened for cloud contamination and snow with the state flags in MOD09A1 and MOD15A2 products, respectively.

2.2. LAI Field Plot Measurements and Fine Resolution LAI Maps

[11] Ground LAI measurements are available for the evaluation of the derived LAI products. These include 45 field plot LAI measurements at 28 global sites from 2000 to 2005 gathered by *Ganguly et al.* [2008b] and 81 fine resolution LAI maps over a network of 41 Benchmark Land Multisite Analysis and Intercomparison of Products (BELMANIP) sites between 2000 and 2004 compiled by *Garrigues et al.* [2008] through a coordinated international effort of the CEOS-WGCV LPV Sub-Group. Among these LAI maps, 39 maps of 29 global BELMANIP sites are available (Table 1). Some of the LAI fine resolution maps provided effective LAI, while true LAI is provided for other sites (Table 1). The field plot LAI from *Ganguly et al.* [2008b] is assumed as true LAI since no detailed description was provided.

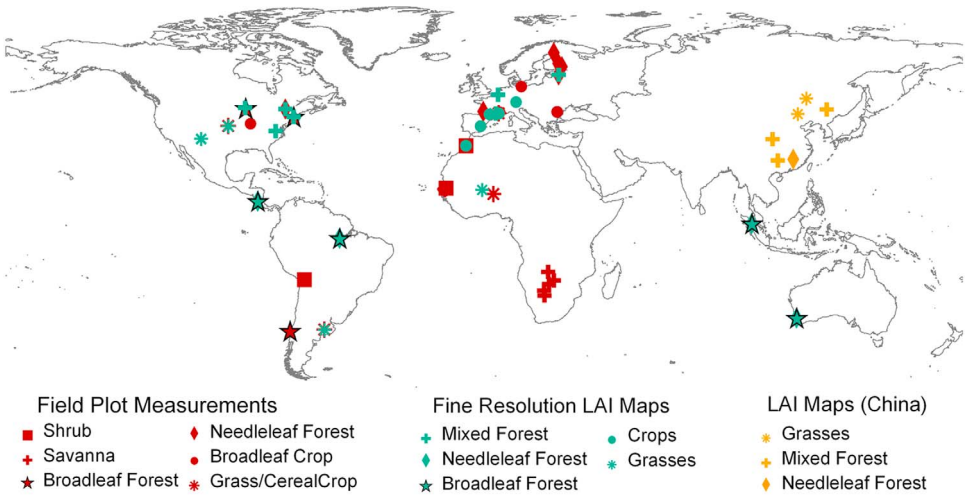

Figure 1. Locations of the LAI field plot measurements and the reference maps used for the MODIS and AVHRR LAI comparison and validation.

[12] In addition, the field LAI data from six sites in China are also used for comparison (Table 1). The LAI was measured in sampling plots with area of about 30 m × 30 m using a LAI-2000 or TRAC instrument with consideration of foliage clumping. Different methods could upscale the plot measurement to scale of satellite product with multi-kilometers resolution in direct validation, such as statistic analysis of the field measurements sampled with consideration of scaling issue [*Privette et al.*, 2002], or generating the fine resolution parameter maps from high-resolution images based on the regression relationships with in situ measurements [*Steinberg et al.*, 2006]. Here, fine-resolution LAI maps were generated with the TM/ETM+ images as a proxy. The clear-sky TM/ETM+ images, which are temporally closest to the field measurements, were georeferenced, radiation corrected, and atmospheric corrected. After that, the TM/ETM+ radiances were converted to spectral reflectances to calculate vegetation indices, such as NDVI, SR, and Reduced Simple Ratio (RSR). The VI values for the sampling plots were used to establish empirical relationships with the field LAI measurements. Then fine-resolution LAI maps with 30 m resolution were generated based on the relationships with best correlation with field LAI measurements. At the Hulunbeier and Xilinhaote sites, the clumping index was assumed to be 1.0 for these grassland regions. At the Maoershan site, the fine resolution effective LAI map was generated on the basis of the empirical relationship between RSR and in situ effective LAI. The vegetated pixels in TM imagery were classified to be coniferous forests, broadleaf forests, and mixed forests. The effective LAI was then converted to the true LAI with the average value of field-measured clumping index for each biome type, which are 0.63 for coniferous forests, 0.83 for broadleaf forests, and 0.75 for mixed forests [*Zhu et al.*, 2010]. These fine resolution LAI maps cover large areas, and the sampling plots may be too sparse to characterize the local vegetation in some regions. The maps around the sampling plots were extracted with a general area of approximately 60–80 km^2 to ensure the reliability of the fine resolution LAI maps. Finally, 45 field plot measurements and 45 fine resolution LAI maps were compared with the retrieved LAI series to evaluate its accuracy. Figure 1 shows the distribution of these ground data.

3. Methodology

3.1. Implementation of the Algorithm

[13] The algorithm includes following steps (Figure 2). First, the MODIS LAI series was derived from the MODIS land surface reflectance data using the GLOBCARBON LAI algorithm [*Deng et al.*, 2006]. Then, the relationship between AVHRR SR and MODIS LAI was established pixel-by-pixel using those MODIS LAI and AVHRR observations during the overlapped period from 2000 to 2006. And then, these pixel-based relationships were applied to historical AVHRR data to estimate LAI series back to 1981. The long-term LAI was made up by combination of AVHRR LAI (1981–2000) and MODIS LAI (2000–2011) after scaling to same spatial and temporal resolution (8 km, half month) by averaging the valid retrievals in each 8 km grid and selecting the valid retrievals with larger LAI values during the composite period.

3.1.1. Retrieval of MODIS LAI Series

[14] A MODIS LAI series (hereinafter referred to as the MODIS LAI) from 2000 to 2011 was derived from the MOD09A1 land surface reflectance and illumination and view angles based on the GLOBCARBON LAI algorithm [*Deng et al.*, 2006], which produces LAI based on the land cover-dependent relationships between LAI and SR as well as RSR with the consideration of BRDF effects explicitly based on the four-scale model and Chebyshev polynomials. First, the effective LAI (L_E) is derived based on the function of SR or RSR:

$$L_E = f_{\mathrm{LE\_SR}}(SR \cdot f_{\mathrm{BRDF}}(\theta_v, \theta_s, \phi)) \tag{1}$$

$$L_E = f_{\mathrm{LE\_RSR}}\left(SR \cdot f_{\mathrm{BRDF}}(\theta_v, \theta_s, \phi) \cdot \left(1 - \frac{\rho_{\mathrm{SWIR}} \cdot f_{\mathrm{SWIR\_BRDF}}(\theta_v, \theta_s, \phi) - \rho_{\mathrm{SWIRmin}}}{\rho_{\mathrm{SWIRmax}} - \rho_{\mathrm{SWIRmin}}}\right)\right) \tag{2}$$

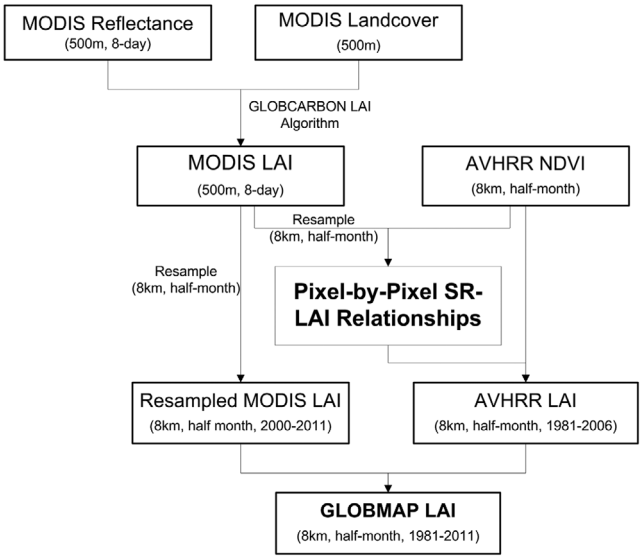

Figure 2. General flowchart for the pixel-based relationship LAI algorithm.

where SR is simple ratio; ρ_{SWIR} is the band 5 (SWIR) reflectance for MODIS; ρ_{SWIRmax} is the maximum value of SWIR reflectance and ρ_{SWIRmin} is the minimum value of SWIR reflectance, both being determined from 1% cutoff points in the histogram of the input SWIR image; $f_{\mathrm{LE\_SR}}$ and $f_{\mathrm{LE\_RSR}}$ are functions defining the relationships between L_E and SR and between L_E and the RSR, which can partly remove the background soil effect [*Brown et al.*, 2000], at a specific view and sun angle combination (θ_v, θ_s, ϕ_s). Functions f_{BRDF} and $f_{\mathrm{SWIR\_BRDF}}$, quantifying the BRDF effects, depend on the angular reflectance behavior of the spectral bands involved.

[15] Then the true LAI is generated from effective LAI retrievals based on the relationship between L_E and the true LAI which is defined as [*Chen et al.*, 2005]

$$\mathrm{LAI} = L_E/\Omega_b \tag{3}$$

where Ω_b is the clumping index for a specific biome *b*.

[16] The IGBP land classes in MCD12Q1 were grouped into six biomes (grasses and cereal crops, conifer, tropical, deciduous, mixed forest and shrub) and one nonvegetated class. The vegetation clumping effect at the plant and canopy scales was accounted for by a land cover-dependent empirical clumping index, which derived from the statistics of the clumping index for global major biomes by *Chen et al.* [2005]. The GLC2000 land classes in statistics of *Chen et al.* [2005] were ground into six biomes, and the mean values of the clumping index for the classes of each biome is averaged, 0.65 for conifer forest, 0.67 for tropical and deciduous forest, 0.69 for mixed forest, 0.71 for shrub, and 0.74 for crop, grass and others.

3.1.2. Establishment of Pixel-Based AVHRR SR–MODIS LAI Relationship

[17] Both GIMMS and MODIS have global measurements from February 2000 to December 2006. Based on these overlapped observations of 7-year period, the pixel-based SR-LAI relationships could be established from the GIMMS NDVI and the MODIS LAI. SR is approximately linearly related with LAI for most biomes [*Chen and Cihlar*, 1996; *Chen et al.*, 2002]. To reduce the uncertainty from the assumption of linear SR-LAI relationship, SR was divided into 10 bins according to the 10 equally sized NDVI bins ranging from 0 to 1.0 at an interval of 0.1. In each bin, the SR-LAI relationship is assumed to be linear. The binned method is flexible to describe various canopy and soil properties for the globe. The pixel-by-pixel SR-LAI relationships were established for each bin from GIMMS NDVI and the coincident MODIS LAI by the following procedures.

[18] 1. The GIMMS NDVI data sets (1981–2006) were converted to SR using

$$\mathrm{SR} = (1 + \mathrm{NDVI})/(1 - \mathrm{NDVI}) \tag{4}$$

[19] 2. The temporal and spatial resolutions of the MODIS LAI and AVHRR SR data sets were scaled to be consistent. The MODIS LAI has a 500 m spatial resolution and an 8 day temporal resolution, while it is 8 km and 15 days for AVHRR SR. The MODIS LAI was scaled to the corresponding temporal and spatial resolution with the AVHRR SR. The MODIS LAI was resampled to an 8 km resolution by averaging the valid retrievals in each 8 km grid. Then, the temporal resolution was reduced to 16 days by selecting the valid retrievals with larger LAI values in the two adjacent MODIS LAI images.

[20] 3. The scaled MODIS LAI and AVHRR SR data were matched in pairs to generate the pixel-specific LAI–SR relationships. For each pixel, the SR-LAI pairs were divided into 10 groups according to SR ranges of [0, 1.22), [1.22, 1.5), [1.5, 1.86), [1.86, 2.33), [2.33, 3), [3, 4), [4, 5.67), [5.67, 9), [9, 19), [19, + ∞). The LAI values in the SR-LAI pairs were normalized to the mean SR value for the middle value of each bin range through linear interpolation. The mean LAI corresponding to the middle value of each bin was calculated as the reference LAI for this bin. For those pixels that vegetation shows regular seasonal variations, there are enough observations to build relationship for most of bins. However, for those that seasonal fluctuation in vegetation is small, the observations is concentrated only on several SR bins. For example, for evergreen vegetation, mainly on those bins approximate to the maximum NDVI; and for semiarid vegetation, mainly on those low SR bins. For those bins without enough valid MODIS LAI values to build the relationship, their corresponding LAI values were regressed from all observations assumed the linear relationship of SR-LAI.

3.1.3. Retrieval of AVHRR LAI Series Back to 1981 Based on Pixel-by-Pixel SR-LAI Relationships

[21] After the pixel-based SR-LAI relationships were established, these relationships were applied to AVHRR SR data to derive the LAI series back to 1981 (hereinafter the AVHRR LAI). For each pixel in the AVHRR SR images, the background LAI values of the two adjacent SR bins closest to the AVHRR SR value were obtained from the SR-LAI relationship. Then the retrieved LAI was determined through linear interpolation. Pixels with a SR less than 1.22 were labeled as nonvegetated and assigned zero LAI values. For those pixels with SR larger than 19, the LAI is set to the reference LAI of the SR bin of [9, 19). Since the clumping effects have been taken into account in MODIS LAI retrieval,

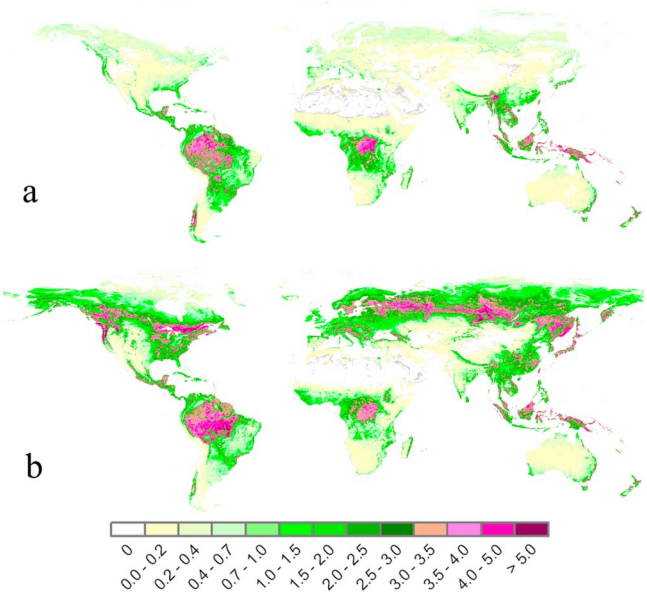

Figure 3. Color-coded maps of the derived global LAI in (a) January 2004 and (b) July 2004.

our LAI series provides true LAI estimation of global vegetation.

3.2. Evaluation of the Consistency of LAI Data Sets

[22] The average state of consistency of the LAI series for a specific location during the statistical period is evaluated by the mean difference (MD(i, j)) for each pixel (i, j), which is defined as

$$\mathrm{MD}(i,j) = \frac{\sum_{t=1}^{N}(\mathrm{AVHRR_{LAI}}(i,j,t) - \mathrm{MODIS_{LAI}}(i,j,t))}{N} \quad (5)$$

Here $\mathrm{AVHRR_{LAI}}$ (i, j, t) and $\mathrm{MODIS_{LAI}}$ (i, j, t) refer to the LAI values derived from AVHRR and MODIS for pixel (i, j) in time t, respectively. N is the total number of the valid LAI values for both AVHRR and MODIS simultaneously.

3.3. Evaluation of Temporal Smoothness

[23] The temporal smoothness of the LAI data sets was quantified by a measure of noise, which was estimated as [*Vermote et al.*, 2009]

$$\mathrm{Noise}(y) = \sqrt{\frac{\sum_{i=1}^{N-2}\left(y_{i+1} - \frac{y_{i+2}-y_i}{\mathrm{day}_{i+2}-\mathrm{day}_i}(\mathrm{day}_{i+1}-\mathrm{day}_i) - y_i\right)^2}{N-2}} \quad (6)$$

where N is the total number of valid LAI values, i refers to a specific LAI in the time series data set, y_{i+1} and y_i are the (i + 1)th and ith LAI values, respectively, and day_{i+1} and day_i are the day numbers corresponding to the (i + 1)th and ith LAI values, respectively.

[24] The LAI was assumed to change linearly between two dates. This linear change hypothesis is valid only when the period is short [*Vermote et al.*, 2009]. Therefore, the noise was computed when LAI values are valid for three continuous composite periods. To avoid the effects of outliers, the 5% of triplets having the largest biases in LAI, which result in large values of the numerator in equation (6), were discarded.

4. Results

4.1. The Long-Term LAI Series Results

[25] Based on this new algorithm, The MODIS LAI series were generated from MODIS data based on the GLOBCARBON LAI algorithm and the AVHRR LAI back to 1981 was estimated from historical AVHRR observations based on the pixel-level relationships. Because the AVHRR LAI is highly consistent with the MODIS LAI (see section 4.2), this LAI product called Long-term Global Mapping LAI (GLOBMAP LAI) over a 30 year period from July 1981 to December 2011 was then made up by combination of AVHRR LAI (1981–2000) and MODIS LAI (2000–2011) with a temporal resolution of half month and a spatial resolution of 8 km.

[26] As examples, the retrieved global AVHRR LAI maps dated January and July 2004 are shown in Figure 3. The data sets reasonably represent the global vegetation characteristics and their seasonal dynamics. The seasonal variations are much more obvious for the region of 30° to 70°N compared with the southern hemisphere and the tropical zone. Deciduous forest and crops are widely distributed in the northern latitudes (30° to 70°N). Due to the changes of radiation and temperature, the vegetation in this region has significant seasonal variations, which are represented by the derived LAI maps. In the tropical zone, the LAI of the evergreen tropical forest is greater than 4 with little seasonal variation. In the southern latitudes (30° to 63°S), the vegetated area is relatively small, resulting in inconspicuous seasonal variations.

4.2. Evaluation of the Consistency of the LAI From AVHRR and MODIS

[27] The AVHRR and MODIS LAI differ in their spatial and temporal resolutions. First, the MODIS LAI was resampled to an 8 km resolution by averaging the valid retrievals in each 8 km grid. Then, its temporal resolution was reduced to 16 days by selecting the larger LAI values in the two adjacent composite dates. The larger values are selected because GIMMS AVHRR data are composed by maximum NDVI selection.

4.2.1. Comparison at the Global Scale

[28] The consistency of the AVHRR and MODIS LAI data sets was evaluated at the global scale by intercomparing statistically the satellite measurements in the overlapped period during 2000–2006. The MD(i, j) were calculated over all vegetated pixels with 8 km data derived from AVHRR and MODIS.

[29] Figure 4 shows the global results of the mean difference between the AVHRR and MODIS LAI for global vegetated regions. Figure 5 presents a histogram of the mean LAI difference. The MD is concentrated on zero with a mean difference of 0.005 and a standard deviation of 0.047 for global vegetated pixels. The difference is within ±0.6 LAI units over 99.0% of the vegetated sites in 2001 based on LAI derived from the SR-LAI relationship established with observations in 2000 and 2002–2006, which indicates the good temporal consistency of the two LAI data sets derived from AVHRR and MODIS observations. This result is somewhat better than

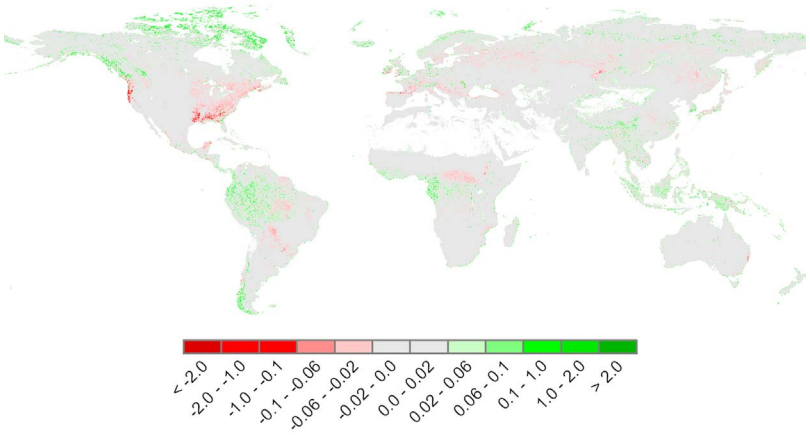

Figure 4. Mean LAI difference between the AVHRR and MODIS LAI from 2000 to 2006.

that of *Ganguly et al.* [2008b], with 96.7% pixels for the same LAI difference range.

[30] Table 2 presents the mean value of the LAI difference (MD_{bio}) and the standard deviation (SD) of the AVHRR LAI with respect to the MODIS LAI for six major biomes. The mean LAI difference is less than 0.01 for the herbaceous biomes, including shrub, grass and crop, while the woody biomes show a mean LAI difference within the range of −0.02 to 0.02 for coniferous forests, deciduous forests, mixed forests and tropical forests. All biomes show a SD within 0.06. The AVHRR LAI slightly underestimates the MODIS LAI for deciduous forest, with a MD of −0.013 and mixed forests of −0.006. In tropical zones, such as the Amazon in South America, tropical Africa, the Congo basin and Indonesia, the LAI difference is approximately ±0.5, with a mean value of 0.02 and a SD of 0.06 because the LAI of dense forests is relatively large in these regions, which would result in a greater difference between the two LAI data sets.

4.2.2. Temporal Consistency at Typical Sites

[31] The AVHRR and MODIS LAI were compared at 352 global BELMANIP vegetated sites during the overlapped period of 2000–2006 to further evaluate the consistency of the two data sets. To minimize the bias of geolocation, the LAI values of 3 × 3 pixels around the site of the same biome with the site were averaged. Figure 6 represents the pixel-by-pixel scatterplot of the two LAI data sets. The plots are close to the 1:1 line, with a slope of 1.01 and an offset of 0.01. The R^2 (0.99) and RMSE (0.11) indicate good agreement between the two data sets. Table 3 presents a statistical analysis for the major biomes. The two LAI data sets are very close for crop and grass, with an R^2 above 0.98 and an RMSE less than 0.1. For woody biomes, including mixed forest, needleleaf forest and deciduous broadleaf forest, the AVHRR LAI agree well with those from MODIS, with an R^2 above 0.94 and an RMSE ranging from 0.13 to 0.14. For evergreen broadleaf forest, the two LAI data sets show somewhat large differences, with an RMSE of 0.19. Its complex vegetation structure may lead to the large difference between the AVHRR and MODIS LAI series.

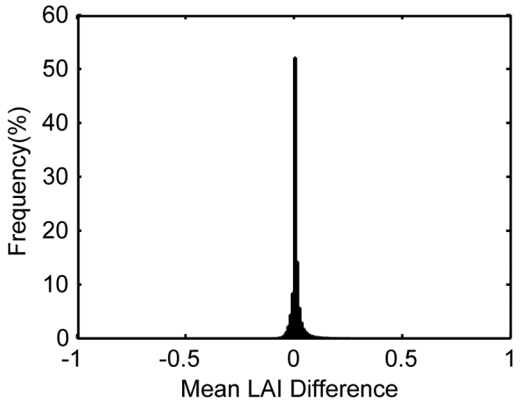

Figure 5. Histogram of mean LAI difference between the AVHRR and MODIS LAI from 2000 to 2006.

[32] The temporal profiles of the LAI time series derived from AVHRR and MODIS were compared over four BELMANIP sites to evaluate the temporal consistency and seasonal variation for four main biomes, including Konza Prairie (KONZ, USA, grassland), Harvard Forest (HARV, USA, deciduous broadleaf forests), Ruokolahti (Finland, needleleaf forests), and SantaRosa (PortoRico, mixed forests). Several ground data throughout the 2000–2003 periods are also presented here. Figure 7 shows the temporal profiles of the AVHRR and MODIS LAI. The seasonality of these four sites is well depicted. The two data sets show good consistency in all four sites, with LAI differences within 0.5 for most pixels. At the SantaRosa site, the derived LAI show some low values during the growing season, which may be due to frequent clouds in this tropical region. The MODIS LAI is somewhat higher than the AVHRR LAI for a few pixels, possibly because the MODIS sensor is more sensitive to flourishing vegetation. Some outliers exist in the LAI series, which can probably be attributed to atmospheric contamination.

Table 2. Global-Scale Analysis of LAI Differences Across Major Biomes

Biome	Conifer Forests	Tropical Forests	Deciduous Forests	Mixed Forests	Shrub	Grass and Crop
MD_{Bio}	0.002	0.017	−0.013	−0.006	0.006	0.004
SD	0.003	0.056	0.039	0.035	0.034	0.035

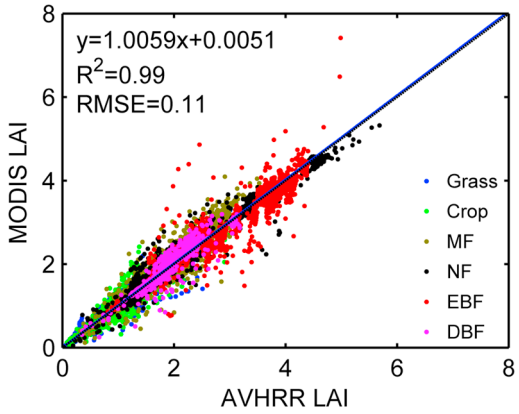

Figure 6. Comparison of the AVHRR and MODIS LAI at 352 global BELMANIP sites.

4.2.3. Evaluation of the Removal of Spectral Inconsistency From Multisensors

[33] The AVHRR and MODIS observations have great differences in spectral characteristics. Here, the characteristics of spectral measurements of the red and NIR bands are represented by the NDVI. The MODIS and AVHRR NDVI, which is equivalent to SR in terms of spectral information, were compared during the overlapped period from February 2000 to December 2006. The MODIS NDVI was resampled to the same spatial resolution of 8 km by averaging valid pixels and the temporal resolutions of 15 days with maximum selection. Statistical analyses were only performed in those vegetated pixels, with MODIS and AVHRR NDVI both above 0.2. In addition, the cloudy pixels labeled by the MOD09 state and the GIMMS NDVI flag were excluded.

[34] Figure 8a presents histograms of the AVHRR and MODIS NDVI, showing that the measurements of MODIS differ significantly from those of AVHRR. Unlike AVHRR NDVI, there are considerably fewer pixels with values less than 0.4 for MODIS NDVI, while there are more pixels with high values above 0.7. For MODIS, the percentage of pixels with NDVI value less than 0.45 is approximately 33.7%, while this percentage is 38.4% for AVHRR. Also, the percentage with an NDVI value greater than 0.70 is above 22.8% for MODIS, in contrast to the 18.3% for AVHRR. Figure 8b shows histograms of the AVHRR and MODIS LAI. For MODIS, the retrieved LAI ranges are 0–2, 2–3.5 and above 3.5 in proportion to 75.0%, 15.2% and 9.8% of the global vegetated pixels, respectively, while they are 74.2%, 17.3% and 8.4% for AVHRR. The two LAI data sets show a good consistency despite the great differences in the measurements as inputs of these two sensors, indicating that our algorithm can remove the inconsistency from multisensor data.

Table 3. Comparison of the AVHRR and MODIS LAI Over 352 BELMANIP Sites

Biome	Crop	Grass	Mixed Forest	Needleleaf Forest	Evergreen Broadleaf Forest	Deciduous Broadleaf Forest
Slope	1.03	1.00	1.05	0.99	0.96	1.02
Offset	−0.01	−0.0003	−0.05	0.05	0.11	0.01
R^2	0.98	0.99	0.95	0.97	0.95	0.94
RMSE	0.08	0.06	0.13	0.14	0.19	0.13

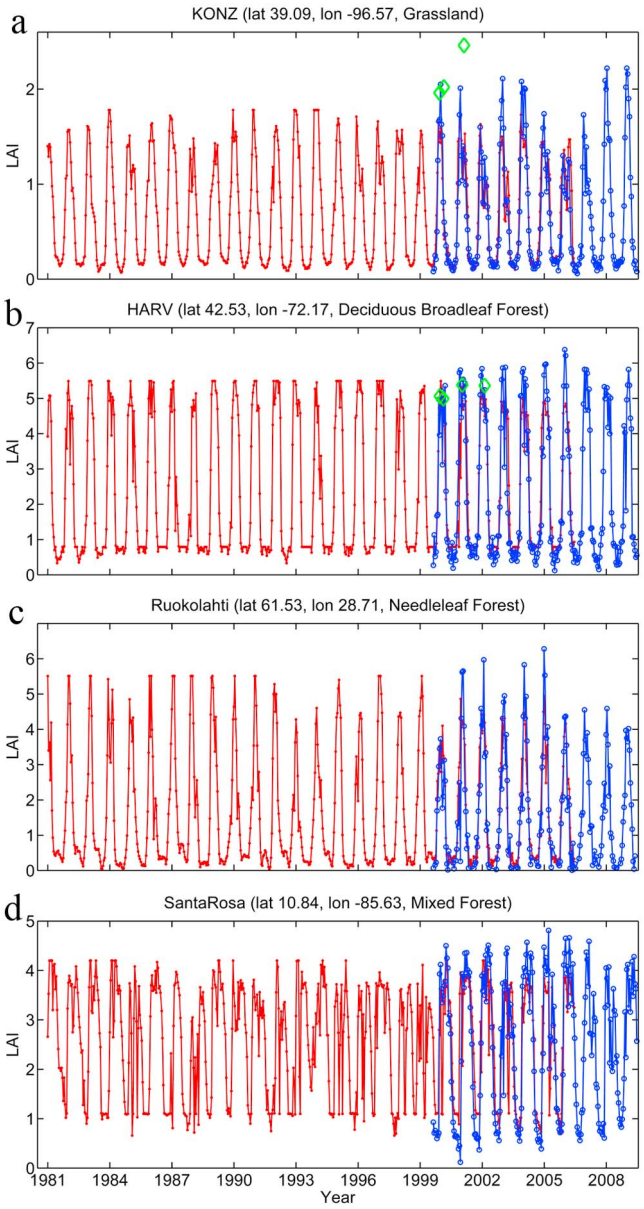

Figure 7. Temporal profiles of the AVHRR LAI from 1981 to 2006 (red line) and MODIS LAI from 2000 to 2009 (blue line) and field measurements (green square) over BELMANIP sites: (a) KONZ grassland site, (b) HARV deciduous broadleaf forest site, (c) Ruokolahti needleleaf forest site, and (d) SantaRosa mixed forest site.

4.3. Comparison With NASA MODIS MOD15A2 C5 LAI Products

[35] The globally retrieved LAI series from AVHRR were compared with the latest version of NASA MODIS MOD15A2 (C5) product for major biome types during the overlapped period of February 2000 to December 2006. Cloudy pixels and pixels from the back-up algorithm for MOD15A2 are screening

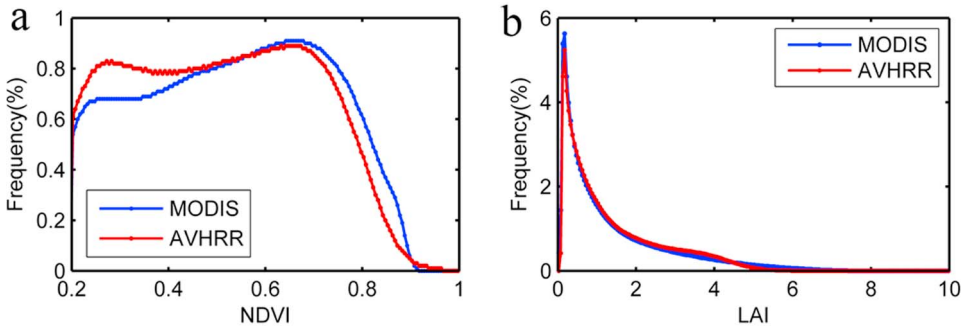

Figure 8. Comparison of NDVI and the derived LAI from AVHRR and MODIS. (a) Histogram of NDVI. (b) Histogram of the derived LAI.

(see section 2.1). After that, the MOD15A2 data sets were aggregated to an 8 km spatial resolution and to a temporal resolution of 16 days with a maximum LAI. Only those pixels with valid LAI values for the MOD15A2 and the AVHRR LAI were included in this comparison.

[36] The histograms of MOD15A2 and the AVHRR LAI for six main biomes are shown in Figure 9. The two data sets show similar shapes while a slight shift toward high values is presented for the MOD15A2 product. There are more pixels with very low LAI values in the derived product for shrub, grasses and crops than that of MOD15A2, which may be due to the soil effects for the sparse vegetation. For tropical forests, the discrepancies among the two data sets are obvious. The two data sets shows similar histogram shapes with different peaks for LAI values (3.8 for AVHRR LAI and 5.0 for MOD15A2 LAI). The high LAI values are mainly concentrated on about 6 for AVHRR LAI and 7 for MOD15A2 LAI. Generally, MOD15A2 products present more pixels with high LAI values than that of our results, and only a few pixels are larger than six for our results, the landscape clumping which is taken into account in MOD15A2 algorithm but not in the GLOBCARBON algorithm may explain part of the lower LAI estimates in the derived product [*Knyazikhin et al.*, 1998; *Deng et al.*, 2006]. For coniferous forest, the derived product shows more pixels with LAI > 3 than that of MOD15A2, which may be due to the different ways in considering the clumping effect.

4.4. Validation With Ground Data

[37] The GLOBMAP LAI was compared with 45 field plot measurements over 28 global sites and 45 fine resolution LAI maps over 29 sites that cover major global biome types. The performance of our pixel-based relationship algorithm was

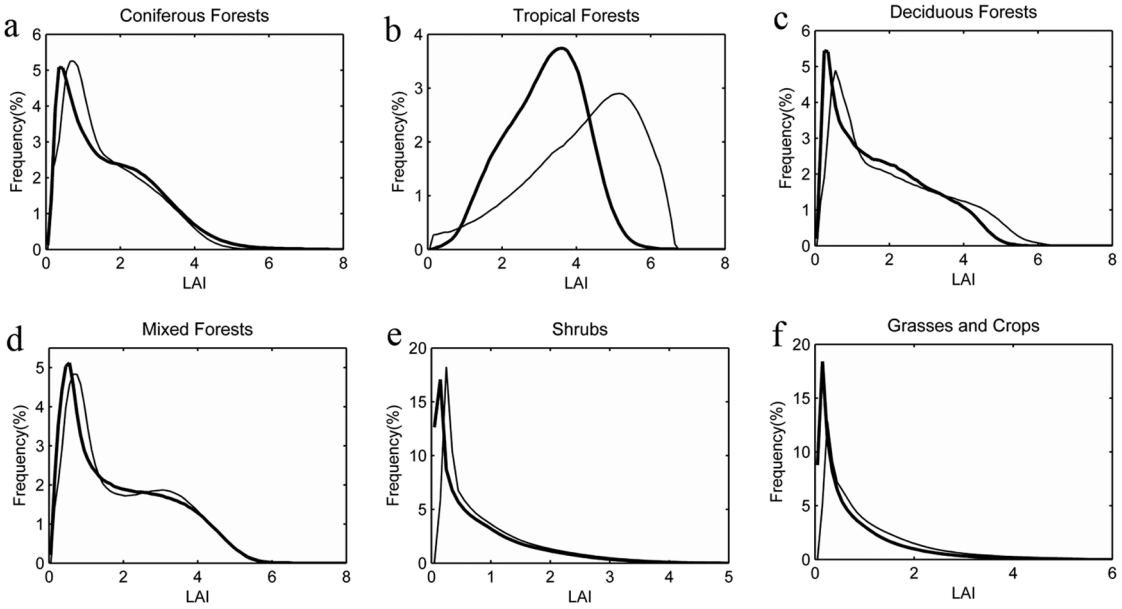

Figure 9. Histogram of the AVHRR LAI (thick solid line) and MOD15A2 (thin solid line) for global vegetated pixels during 2000–2006. (a) Coniferous forests, (b) tropical forests, (c) deciduous forests, (d) mixed forests, (e) shrubs, and (f) grasses and crops. Only the main algorithm is considered here for MOD15A2.

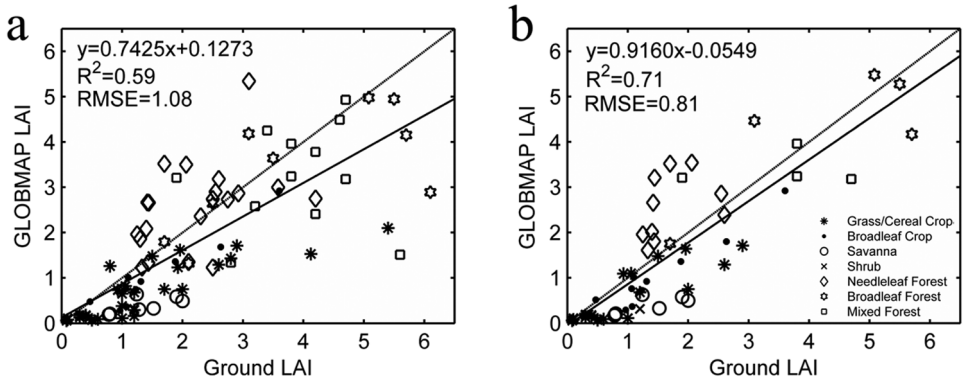

Figure 10. Comparison of the derived LAI and ground LAI data: (a) results with all ground data available and (b) results that exclude the ground data if the MOD12 land cover type differs from the field definition or the clumping effects were not corrected.

evaluated by the AVHRR LAI before 2006 and MODIS LAI after 2007.

[38] Comparing satellite LAI data sets with spatial resolutions from several hundreds of meters to kilometers with field measurements is complex due to the uncertainties from scaling, heterogeneity, geolocation, and the limited spatial and temporal sampling of ground data, among other factors [*Privette et al.*, 2000; *Weiss et al.*, 2007]. To reduce the uncertainties of these factors, the LAI retrievals on 3 × 3 pixels around the site were averaged and then compared with the field plot measurements. In contrast, fine resolution LAI maps are generated based on the regression relationship between field measurements and vegetation indices in high-resolution images, such as Landsat TM/ETM+, SPOT and ASTER. These LAI maps are then aggregated to the same resolution with the retrieved LAI so that the effects of spatial scaling and the heterogeneity of the land surface can be greatly reduced. The typical extent of these maps is approximately 9–100 km^2. For each site, the LAI value for the pixel covers most area of the site in the image which is temporally closest to the field measurements was directly compared with the average value of the fine resolution LAI map. Figure 10a presents the pixel-by-pixel comparison of these two data sets. The GLOBMAP LAI explains 59% of the variability in ground LAI and is biased by 1.08 LAI on average.

[39] The MOD12 land cover product is one of inputs in generation of LAI from MODIS observations. The misclassification in the input MOD12 land cover map would result in large bias in LAI estimation [*Liu et al.*, 2007]. To focus on evaluation of the uncertainties of our algorithm, those retrievals were excluded if the land cover type of MOD12 mismatch with that of the field observations to eliminate the uncertainties due to land cover maps misclassification. Besides, some of the LAI fine resolution maps provided effective LAI (Table 1). Since our product provides true LAI by accounting vegetation clumping effects using land cover-dependent clumping index (see section 3.1.1), these effective LAI maps were excluded in final comparison. The field plot LAI from *Ganguly et al.* [2008b] is assumed as true LAI and compared directly with derived LAI. As a result, 38 field plot measurements over 24 global sites and 19 reference maps over 11 global sites (including 5 BELMANIP sites) were selected for comparison. Figure 10b shows results of the comparison of the two data sets. The GLOBMAP LAI and the ground data are close to the 1:1 line, with a slope of 0.92 and an offset of −0.05. The RMSE decreases from 1.08 to 0.81 and the R^2 increases from 0.59 to 0.71. The retrieved results generally agree well with the ground data for grass, cereal crop, broadleaf crop, broadleaf forest and mixed forest, with plots close to the 1:1 line. The GLOBMAP LAI underestimates low LAI values for grass, crop, savanna and shrub, which may due to the influence of soil effects of sparse vegetation. For crops, the GLOBMAP LAI underestimates the ground data for those at approximately 3, which may be attributed to the uncertainties from the high heterogeneity of croplands. Additionally, the model parameters for crop type used to generate LAI may not correspond well with the characteristics of dense crops. Our algorithm overestimates the LAI of coniferous forests with significant clumping phenomenon, which may due to the uncertainties of empirical land cover-dependent clumping index employed in transferring of effective LAI to true LAI.

4.5. Comparison With the LAI Retrieved Directly From AVHRR Data

[40] The AVHRR LAI was compared with the LAI directly retrieved from AVHRR data based on the GLOBCARBON LAI algorithm [*Liu et al.*, 2010] (hereafter referred to as direct AVHRR LAI) for a 26 year period from 1981 to 2006. The temporal smoothness of the two LAI series was evaluated with the noise. The accuracy is defined as the bias of the retrieved LAI and the ground LAI measurements. The accuracy of the direct AVHRR LAI was evaluated and then compared with that of the AVHRR LAI.

4.5.1. Comparison of the Temporal Smoothness

[41] The temporal smoothness of the AVHRR LAI and the direct AVHRR LAI were evaluated with the noise calculated from 1981 to 2006. The noise of the two data sets was calculated for vegetated pixels, and only those pixels with valid noise estimation for both LAI series were included in the statistical analysis. Figure 11 shows a histogram of the noise of the two LAI sequences. The noise for the AVHRR LAI is concentrated on zero, with an average value of 0.14, while it is much larger for the direct AVHRR LAI series, with average noise value of 0.32. Thus, our method can decrease the

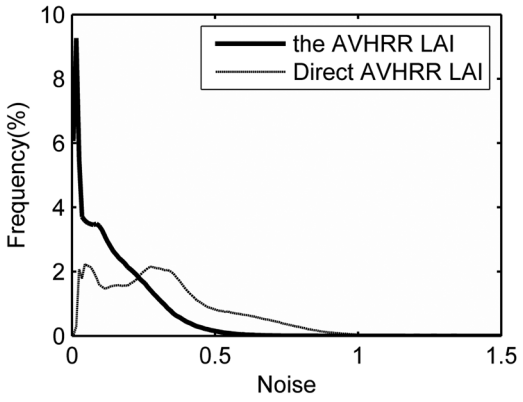

Figure 11. Histogram comparison of the noise of the two AVHRR LAI data sets based on the GLOBCARBON LAI algorithm and the pixel-based SR-LAI relationship method.

temporal noise by 56%, which suggests that this method can improve the quality of retrievals from low-quality inputs.

4.5.2. Comparison of Accuracy

[42] The accuracy of the direct AVHRR LAI was also evaluated through validation against field plot measurements and fine resolution LAI maps acquired before December 2006 (section 2.2). Retrievals and ground data were only included if the MOD12 land cover type agreed with the field observation and the clumping effects were corrected. Figure 12 presents the results. The plots are dispersive with an RMSE of 1.65, which is much larger than that of the AVHRR LAI (0.81). Thus, our method can decrease the RMSE by approximately 51%. The R^2 of the direct AVHRR LAI is 0.36, which is less than that of the AVHRR LAI (0.71). It is suggested that the pixel-based SR-LAI relationship method could help to improve the accuracy of LAI retrieved from low-quality historical AVHRR observations by using the high-quality LAI produced from MODIS as constraints.

5. Discussion

[43] It is challenging to generate such a multidecade time series that spans several sensors. The differences of spectral response function, data quality and band information content should be the causes of inconsistency between products from different sensor data. The differences of spectral response function could be lessened by physically based radiative transfer approach [*Ganguly et al.*, 2008a]. However, it is difficult to account for the differences for diverse vegetation of the globe using a radiative transfer model with limited constraints from remote sensing. Moreover, the low-quality and limited spectral bands of historical AVHRR hamper direct retrieval of LAI from the reflectances based on radiative transfer method. The discrepancy of data quality for different input would also lead to inconsistency of products. In this paper, the pixel-based AVHRR SR-MODIS LAI relationships were established from overlapping observations and applied for AVHRR retrieval. Thus, the consistency of the long-term LAI data set is improved by establishing the direct relationship between MODIS and AVHRR data. Since this relationship is established pixel-by-pixel, this VI-based approach could be applied to the globe with accounting for the differences of canopy shapes, understory vegetation composition, moisture and soil properties for global sites. Because the SR is more reliable than reflectances for low-quality data, the input as SR would improve the AVHRR LAI quality. And the SR-LAI relationships were established by the LAI derived from MODIS that means that the retrieval of AVHRR LAI is constrained by MODIS observations with high quality, which helps to improve the LAI retrieval from low-quality AVHRR data.

[44] The relationship between VI and LAI can be described by mathematical model or binned method. The former prescribes a mathematical form of the SR-LAI relationship in whole value range, such as linear, logarithmic or polynomial models. Although the parameters of the model may vary with pixels, it is hard to find a prescriptive model suitable for all vegetation over the globe. The latter actually generates the look-up table between LAI and VI for each pixel. Without assuming the functional form between the VI and LAI in whole value range, this method is more flexible to characterize diverse canopy and soil properties at the global scale. Although the assumption of linearity relationship between SR and LAI in each bin may introduce uncertainties of the results, this binned method could partly reduce its influence with more bin ranges.

[45] Optical remote sensing measurements made at a single angle provide information of the effective LAI, taken as the product of LAI and the clumping index [*Chen*, 1996]. The observed disparity between the derived LAI and MOD15A2 as well as ground data could be partly attributed to the differing definition of LAI, especially the various mechanisms in considering the clumping effects. The GLOBCABON and MOD15 LAI algorithm both estimate LAI, but the clumping effects are considered in different ways in canopy structure modeling. The GLOBCARON LAI algorithm accounts for the clumping effects of vegetation at plant/shoot and canopy scales by a land cover-dependent empirical clumping index, while MOD15 algorithm considers the vegetation clumping at plant/shoot and canopy scales through 3D radiative transfer formulations, and the clumping at the landscape scale is partly addressed through mechanisms based on the radiative transfer theory of canopy spectral invariants [*Knyazikhin et al.*, 1998]. These discrepancies probably result in larger

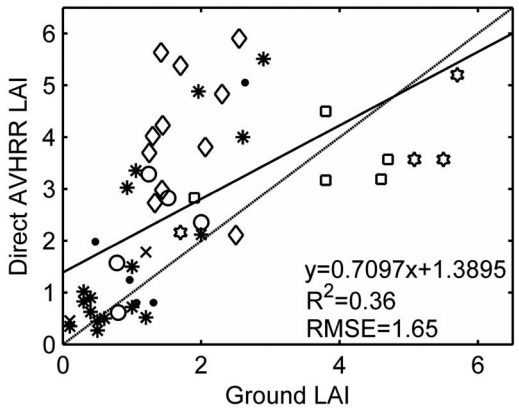

Figure 12. Comparison of direct AVHRR LAI against ground LAI data (for legend, see Figure 10).

MOD15 LAI values than that of GLOBCABON LAI for major biomes [*Garrigues et al.*, 2008] and may also explain part of the lower LAI estimates of our algorithm. For ground data, the various measurements methods provide LAI with different meanings. LAI obtained from the direct measurement methods and the allometric method generally are considered as true LAI. While measurements obtained from the indirect optical methods without clumping correction correspond to the effective LAI derived from measured canopy gap fraction. Although the foliage clumping effects have been accounted for at some sites with the TRAC instrument, such as the six sites in China, some of the ground data are the effective LAI. The effective LAI have been excluded to lessen its influence, but the empirical land cover-dependent clumping index employed in our algorithm may also introduce uncertainties in comparison results for diverse vegetation in the field sites.

[46] Several factors may introduce uncertainties to the GLOBMAP LAI data set, such as land cover, land cover change, atmospheric effect, and BRDF effect. Since vegetation structure is distinctly different among land cover types, the land cover map is a critical input in LAI retrieval [*Liu et al.*, 2007]. In the GLOBCARBON LAI algorithm, the functions of LAI and SR/RSR considerably differ among land cover types according to simulations of four-scale model [*Deng et al.*, 2006]. The MOD12 land cover product is one of inputs in generation of the MODIS LAI which is the base of the AVHRR SR-LAI relationship. Since the AVHRR LAI is retrieved from this MODIS LAI data set, the accuracy of the input MCD12Q1 land cover map would affect LAI estimation of our algorithm.

[47] Land cover change is another source of uncertainties. In our algorithm, it is assumed that the LAI–SR relationship is stable throughout the processing period. If the land cover changes during this period, this SR-LAI relationship may change and introduce uncertainties in the LAI retrieval from AVHRR. However, this land cover change may introduce little uncertainty for most situations. If the vegetation was destroyed, the vegetation became sparse with low SR value, so the SR-LAI relationship will also be applicable. If the forests change into grassland or crops, the SR-LAI relationship may somewhat change. But the vegetation index (SR) will largely decrease in that case, and the change of SR-LAI relationship will have little effect on LAI retrieval because the vegetation index can represent the vegetation regrowth to the first order of accuracy. In contrast, the retrieval may be greatly affected if the land cover changes happen between different forest types, especially conversion between broadleaf and conifer vegetation. However, this type of chances may not be common.

[48] Due to the limited number of bands of AVHRR, it is difficult to correct the atmospheric effects in AVHRR observations. No atmospheric correction is performed for the GIMMS NDVI data sets, except for the stratospheric aerosol produced by the El Chinchon and Mt. Pinatubo volcanic periods. The GIMMS NDVI is the maximum NDVI selection in the compositing period, and the SR can lessen the atmospheric effects. Even so, atmospheric effects still cannot be removed completely and may introduce uncertainties in SR-LAI relationships and LAI retrieval from AVHRR observations.

[49] The BRDF effects would have also played a role in LAI retrieval from AVHRR directional land surface reflectance. The 55° sensor swath width and the variable solar angle result in variable illumination and view angles of AVHRR measurements. Besides, the overpass times of NOAA AVHRR satellites series used for GIMMS NDVI generation drifted by 1–2 min per month to as much as 4.5 h later in the day, creating variable Sun-target-sensor geometry over the period of record [*Tucker et al.*, 2005]. Although the solar zenith angle and viewing angle effects due to satellite drift have been corrected based on the Empirical Mode Decomposition (EMD) algorithm [*Pinzon et al.*, 2004], BRDF normalization is not performed in GIMMS NDVI data sets. Due to the limited angular sampling and low data quality, it is hard to retrieve BRDF parameters based on AVHRR data. A long period of acquisition is generally required to obtain clear-sky multiangle measurements. However, it is not guaranteed that the BRDF of vegetation remains constant over time, and atmospheric conditions can vary considerably [*Shepherd and Dymond*, 2000]. Thus, angular normalization probably introduces uncertainties in LAI retrieval. Several attempts have been made to reduce the influence of BRDF effects in our algorithm. SR could partially reduce the influence of BRDF effects because of the correlation between red and NIR reflectances [*Chen*, 1996]. Additionally, as pixel-level SR-LAI relationships is established from the multiyear observations, the influence of BRDF effects may be partially counteracted based on these measurements on various illumination and view angles for each pixel.

[50] The performance of our algorithm may be improved by employing a better mechanism in considering the clumping effect. Global foliage clumping index map has been generated based on multiangular POLDER data [*Chen et al.*, 2005]. Since the GLOBCARBON LAI algorithm accounts for vegetation clumping at the plant and canopy scales by application of a land cover-specific clumping index, the uncertainties in derived LAI series could be reduced with consideration of the clumping effect at the pixel level by employing global clumping index map. BRDF and atmospheric effects of AVHRR data are major factors that affect the performance of the algorithm. Combination with other sensors may help to correct atmospheric and BRDF effects of AVHRR data [*Los et al.*, 2005]. The high-quality observations from MODIS during the overlapping period may also provide constraints for atmosphere and BRDF parameters inversion. The performance of our algorithm may be improved with better AVHRR surface reflectance data with more elaborate atmospheric correction, calibration, geolocation and angular normalization. With development of remote sensing, more and more physical and biochemical parameters of vegetation and land surface may be mapped. With these parameters as constraints, the physical radiative transfer model may be performed better for each pixel, and the historical low-quality observations may be better processed.

6. Conclusion

[51] An approach for generating a consistent long time series (1981–2011) of LAI products through the combination of MODIS and historical AVHRR data is presented. The consistency of the long-term LAI data set from multisensors is a critical issue because of the significant differences of many factors, such as the spectral response function and band information content. Our algorithm addresses this issue by establishing pixel-by-pixel relationships between MODIS

and AVHRR observations. This approach ensures the consistency of retrievals from these two different sensors and helps to reduce the uncertainties introduced from the low-quality and limited band information of AVHRR observations.

[52] The long-term LAI derived from AVHRR was compared with that from MODIS during the overlapped period from 2000 to 2006. Although there are significant differences between MODIS and AVHRR observations due to their variations in spectral response function and other characteristics, the two derived LAI data sets show a good consistency. Intercomparisons between them show that pixels within a ± 0.6 LAI difference constitute 99.0% of the total global vegetated regions, with a mean difference of 0.005. A comparison of the AVHRR and MODIS LAI at 352 global BELMANIP sites also indicates a good agreement, with an RMSE value of 0.11 LAI. The derived AVHRR LAI series shows a similar statistical distribution of LAI values with the NASA MODIS MOD15A2 LAI products for global major vegetation types. The results were also validated against field measurements and fine resolution LAI maps. After excluding the uncertainties of the input land cover map and clumping effects, the long-term LAI could explain 71% of the variability in the ground LAI over global sites covering all major vegetation types, and it was biased by 0.81 on average. Compared with the method directly retrieving LAI from AVHRR data based on the GLOBCARBON LAI algorithm, the pixel-based SR-LAI relationship method decreased the temporal noise of the LAI series from AVHRR by 56%, from 0.32 to 0.14, and decreased the RMSE by approximately 51%, from 1.65 to 0.81, compared with the ground data with constraints from high-quality MODIS data.

[53] **Acknowledgments.** This research was funded by the China 973 program (2010CB950701), the R&D Special Fund for Public Welfare Industry (meteorology) (GYHY201106014) and the National Natural Science Foundation from China (41171285). GIMMIS NDVI data were downloaded from the Global Land Cover Facility (http://www.glcf.umd.edu/data/gimms/) and MODIS data from the Land Processes Distributed Active Archive Center. We thank the CEOS LPV group for providing ground validation data on their Web site (http://lpvs.gsfc.nasa.gov/LPV_LAI10km.html). We gratefully acknowledge Hongliang Fang for providing many valuable suggestions and Weimin Ju, Yibo Liu, Gaolong Zhu, Bailing Xing, and Jingfang Zhu of Nanjing University for contributions to the field LAI measurements and fine-resolution LAI maps processing in China. The authors also would like to thank the anonymous reviewers for their insightful and critical comments, which make this paper be improved largely. This LAI product is hosted on http://www.globalmapping.org/globalLAI for free download.

References

Abuelgasim, A. A., R. A. Fernandes, and S. G. Leblanc (2006), Evaluation of national and global LAI products derived from optical remote sensing instruments over Canada, *IEEE Trans. Geosci. Remote Sens.*, *44*(7), 1872–1884, doi:10.1109/TGRS.2006.874794.

Aparicio, N., D. Villegas, J. L. Araus, J. Casadesus, and C. Royo (2002), Relationship between growth traits and spectral vegetation indices in durum wheat, *Crop Sci.*, *42*(5), 1547–1555, doi:10.2135/cropsci2002.1547.

Bacour, C., F. Baret, D. Beal, M. Weiss, and K. Pavageau (2006), Neural network estimation of LAI, fAPAR, fCover and LAIxC(ab), from top of canopy MERIS reflectance data: Principles and validation, *Remote Sens. Environ.*, *105*(4), 313–325, doi:10.1016/j.rse.2006.07.014.

Baret, F., and G. Guyot (1991), Potentials and limits of vegetation indexes for LAI and APAR assessment, *Remote Sens. Environ.*, *35*(2–3), 161–173, doi:10.1016/0034-4257(91)90009-U.

Baret, F., et al. (2007), LAI, fAPAR and fCover CYCLOPES global products derived from VEGETATION—Part 1: Principles of the algorithm, *Remote Sens. Environ.*, *110*(3), 275–286, doi:10.1016/j.rse.2007.02.018.

Braswell, B. H., D. S. Schimel, E. Linder, and B. Moore III (1997), The response of global terrestrial ecosystems to interannual temperature variability, *Science*, *278*, 870–873, doi:10.1126/science.278.5339.870.

Brown, L., J. M. Chen, S. G. Leblanc, and J. Cihlar (2000), A shortwave infrared modification to the simple ratio for LAI retrieval in boreal forests: An image and model analysis, *Remote Sens. Environ.*, *71*(1), 16–25, doi:10.1016/S0034-4257(99)00035-8.

Chen, J. M. (1996), Evaluation of vegetation indices and a modified simple ratio for boreal applications, *Can. J. Remote Sens.*, *22*, 229–242.

Chen, J. M., and T. A. Black (1992), Defining leaf-area index for non-flat leaves, *Plant Cell Environ.*, *15*(4), 421–429, doi:10.1111/j.1365-3040.1992.tb00992.x.

Chen, J. M., and J. Cihlar (1996), Retrieving leaf area index of boreal conifer forests using Landsat TM images, *Remote Sens. Environ.*, *55*(2), 153–162, doi:10.1016/0034-4257(95)00195-6.

Chen, J. M., et al. (2002), Derivation and validation of Canada-wide coarse-resolution leaf area index maps using high-resolution satellite imagery and ground measurements, *Remote Sens. Environ.*, *80*(1), 165–184, doi:10.1016/S0034-4257(01)00300-5.

Chen, J. M., C. H. Menges, and S. G. Leblanc (2005), Global mapping of foliage clumping index using multi-angular satellite data, *Remote Sens. Environ.*, *97*(4), 447–457, doi:10.1016/j.rse.2005.05.003.

Chen, X. F., J. M. Chen, S. Q. An, and W. M. Ju (2007), Effects of topography on simulated net primary productivity at landscape scale, *J. Environ. Manage.*, *85*(3), 585–596, doi:10.1016/j.jenvman.2006.04.026.

Ciais, P., et al. (2005), Europe-wide reduction in primary productivity caused by the heat and drought in 2003, *Nature*, *437*(7058), 529–533, doi:10.1038/nature03972.

Cohen, W. B., et al. (2006), MODIS land cover and LAI collection 4 product quality across nine sites in the western hemisphere, *IEEE Trans. Geosci. Remote Sens.*, *44*(7), 1843–1857, doi:10.1109/TGRS.2006.876026.

Deng, F., J. M. Chen, S. Plummer, M. Z. Chen, and J. Pisek (2006), Algorithm for global leaf area index retrieval using satellite imagery, *IEEE Trans. Geosci. Remote Sens.*, *44*(8), 2219–2229, doi:10.1109/TGRS.2006.872100.

Diner, D. J., et al. (2008), MISR level 2 surface retrieval algorithm theoretical basis, Jet Propul. Lab., Calif. Inst. of Technol., Pasadena.

Fava, F., R. Colombo, S. Bocchi, M. Meroni, M. Sitzia, N. Fois, and C. Zucca (2009), Identification of hyperspectral vegetation indices for Mediterranean pasture characterization, *Int. J. Appl. Earth Obs. Geoinf.*, *11*(4), 233–243, doi:10.1016/j.jag.2009.02.003.

Ganguly, S., M. A. Schull, A. Samanta, N. V. Shabanov, C. Milesi, R. R. Nemani, Y. Knyazikhin, and R. B. Myneni (2008a), Generating vegetation leaf area index earth system data record from multiple sensors. Part 1: Theory, *Remote Sens. Environ.*, *112*(12), 4333–4343, doi:10.1016/j.rse.2008.07.014.

Ganguly, S., A. Samanta, M. A. Schull, N. V. Shabanov, C. Milesi, R. R. Nemani, Y. Knyazikhin, and R. B. Myneni (2008b), Generating vegetation leaf area index Earth system data record from multiple sensors. Part 2: Implementation, analysis and validation, *Remote Sens. Environ.*, *112*(12), 4318–4332, doi:10.1016/j.rse.2008.07.013.

Garrigues, S., et al. (2008), Validation and intercomparison of global leaf area index products derived from remote sensing data, *J. Geophys. Res.*, *113*, G02028, doi:10.1029/2007JG000635.

Gitelson, A. A., and Y. J. Kaufman (1998), MODIS NDVI optimization to fit the AVHRR data series spectral considerations, *Remote Sens. Environ.*, *66*(3), 343–350, doi:10.1016/S0034-4257(98)00065-0.

Global Climate Observing System (2006), Systematic observation requirements for satellite-based products for climate, *Tech. Doc. WMO/TD 1338*, 103 pp., World Meteorol. Organ., Geneva, Switzerland. [Available at http://www.wmo.ch/web/gcos/gcoshome.html.]

Heimann, M., and M. Reichstein (2008), Terrestrial ecosystem carbon dynamics and climate feedbacks, *Nature*, *451*(7176), 289–292, doi:10.1038/nature06591.

Heiskanen, J. (2006), Estimating aboveground tree biomass and leaf area index in a mountain birch forest using ASTER satellite data, *Int. J. Remote Sens.*, *27*(6), 1135–1158, doi:10.1080/01431160500353858.

Iiames, J. S., A. N. Pilant, and T. E. Lewis (2004), In-situ estimates of forest LAI for MODIS data validation, in *Remote Sensing and GIS Accuracy Assessment*, edited by R. S. Lunetta and J. G. Lyon, pp. 41–57, CRC Press, Boca Raton, Fla., doi:10.1201/9780203497586.ch4.

Kalacska, M., et al. (2004), Leaf area index measurements in a tropical moist forest: A case study from Costa Rica, *Remote Sens. Environ.*, *91*(2), 134–152, doi:10.1016/j.rse.2004.02.011.

Knyazikhin, Y., J. V. Martonchik, R. B. Myneni, D. J. Diner, and S. W. Running (1998), Synergistic algorithm for estimating vegetation canopy leaf area index and fraction of absorbed photosynthetically active

radiation from MODIS and MISR data, *J. Geophys. Res.*, *103*(D24), 32,257–32,275, doi:10.1029/98JD02462.

Kraus, T., M. Schmidt, S. W. Dech, and C. Samimi (2009), The potential of optical high resolution data for the assessment of leaf area index in east African rainforest ecosystems, *Int. J. Remote Sens.*, *30*(19), 5039–5059, doi:10.1080/01431160903022878.

Leuning, R., Y. Q. Zhang, A. Rajaud, H. Cleugh, and K. Tu (2008), A simple surface conductance model to estimate regional evaporation using MODIS leaf area index and the Penman-Monteith equation, *Water Resour. Res.*, *44*, W10419, doi:10.1029/2007WR006562.

Li, X. F., W. M. Ju, S. Chen, and Y. L. Zhou (2010), Influence of land cover data on regional forest leaf area index inversion, *J. Remote Sens.*, *14*(5), 974–989.

Liu, R., J. M. Chen, J. Liu, F. Deng, and R. Sun (2007), Application of a new leaf area index algorithm to China's landmass using MODIS data for carbon cycle research, *J. Environ. Manage.*, *85*(3), 649–658, doi:10.1016/j.jenvman.2006.04.023.

Liu, S. L., R. G. Liu, and Y. Liu (2010), Spatial and temporal variation of global LAI during 1981–2006, *J. Geogr. Sci.*, *20*(3), 323–332, doi:10.1007/s11442-010-0323-6.

Liu, Y. B., et al. (2011), Retrieval of leaf area index for different grasslands in Inner Mongolia prairie using remote sensing data, *Acta Ecol. Sin.*, *31*, 5159–5170.

Los, S. O., et al. (2000), A global 9-yr biophysical land surface dataset from NOAA AVHRR data, *J. Hydrometeorol.*, *1*(2), 183–199, doi:10.1175/1525-7541(2000)001<0183:AGYBLS>2.0.CO;2.

Los, S. O., P. R. J. North, W. M. F. Grey, and M. J. Barnsley (2005), A method to convert AVHRR normalized difference vegetation index time series to a standard viewing and illumination geometry, *Remote Sens. Environ.*, *99*, 400–411, doi:10.1016/j.rse.2005.08.017.

Masson, V., J. L. Champeaux, F. Chauvin, C. Meriguer, and R. Lacaze (2003), A global database of land surface parameters at 1 km resolution in meteorological and climate models, *J. Climatol.*, *16*, 1261–1282, doi:10.1175/1520-0442-16.9.1261.

Myneni, R. B., et al. (2002), Global products of vegetation leaf area and fraction absorbed PAR from year one of MODIS data, *Remote Sens. Environ.*, *83*(1–2), 214–231, doi:10.1016/S0034-4257(02)00074-3.

Piao, S., P. Ciais, P. Friedlingstein, N. de Noblet-Ducoudré, P. Cadule, N. Viovy, and T. Wang (2009), Spatiotemporal patterns of terrestrial carbon cycle during the 20th century, *Global Biogeochem. Cycles*, *23*, GB4026, doi:10.1029/2008GB003339.

Pinzon, J., M. E. Brown, and C. J. Tucker (2004), Satellite time series correction of orbital drift artifacts using empirical mode decomposition, in *Hilbert-Huang Transform: Introduction and Applications*, edited by N. Huang, pp. 167–186, World Sci., Hackensack, N. J.

Privette, J. L., G. P. Asner, J. Conel, K. F. Huemmrich, R. Olson, A. Rango, A. F. Rahman, K. Thome, and E. A. Walter-Shea (2000), The EOS prototype validation exercise (PROVE) at Jornada: Overview and lessons learned, *Remote Sens. Environ.*, *74*(1), 1–12, doi:10.1016/S0034-4257(00)00117-6.

Privette, J. L., R. B. Myneni, Y. Knyazikhin, M. Mukelabai, G. Roberts, Y. Tian, Y. Wang, and S. G. Leblanc (2002), Early spatial and temporal validation of MODIS LAI product in the Southern Africa Kalahari, *Remote Sens. Environ.*, *83*(1–2), 232–243, doi:10.1016/S0034-4257(02)00075-5.

Shepherd, J. D., and J. R. Dymond (2000), BRDF correction of vegetation in AVHRR imagery, *Remote Sens. Environ.*, *74*(3), 397–408, doi:10.1016/S0034-4257(00)00131-0.

Spanner, M., L. Johnson, J. Miller, R. McCreight, J. Freemantle, J. Runyon, and P. Gong (1994), Remote-sensing of seasonal leaf-area index across the Oregon transect, *Ecol. Appl.*, *4*(2), 258–271, doi:10.2307/1941932.

Steinberg, D. C., S. J. Goetz, and E. J. Hyer (2006), Validation of MODIS F-PAR products in boreal forests of Alaska, *IEEE Trans. Geosci. Remote Sens.*, *44*(7), 1818–1828, doi:10.1109/TGRS.2005.862266.

Tarnavsky, E., S. Garrigues, and M. E. Brown (2008), Multiscale geostatistical analysis of AVHRR, SPOT-VGT, and MODIS global NDVI products, *Remote Sens. Environ.*, *112*, 535–549, doi:10.1016/j.rse.2007.05.008.

Trishchenko, A. P., J. Cihlar, and Z. Q. Li (2002), Effects of spectral response function on surface reflectance and NDVI measured with moderate resolution satellite sensors, *Remote Sens. Environ.*, *81*(1), 1–18, doi:10.1016/S0034-4257(01)00328-5.

Tucker, C. J., J. E. Pinzon, M. E. Brown, D. A. Slayback, E. W. Pak, R. Mahoney, E. F. Vermote, and N. El Saleous (2005), An extended AVHRR 8-km NDVI dataset compatible with MODIS and SPOT vegetation NDVI data, *Int. J. Remote Sens.*, *26*(20), 4485–4498, doi:10.1080/01431160500168686.

Vermote, E., C. O. Justice, and F. M. Breon (2009), Towards a generalized approach for correction of the BRDF effect in MODIS directional reflectances, *IEEE Trans. Geosci. Remote Sens.*, *47*(3), 898–908, doi:10.1109/TGRS.2008.2005977.

Weiss, M., F. Baret, S. Garrigues, and R. Lacaze (2007), LAI and fAPAR CYCLOPES global products derived from VEGETATION. Part 2: Validation and comparison with MODIS collection 4 products, *Remote Sens. Environ.*, *110*(3), 317–331, doi:10.1016/j.rse.2007.03.001.

Yang, W. Z., et al. (2006), MODIS leaf area index products: From validation to algorithm improvement, *IEEE Trans. Geosci. Remote Sens.*, *44*(7), 1885–1898, doi:10.1109/TGRS.2006.871215.

Zhang, K., J. S. Kimball, R. R. Nemani, and S. W. Running (2010), A continuous satellite-derived global record of land surface evapotranspiration from 1983 to 2006, *Water Resour. Res.*, *46*, W09522, doi:10.1029/2009WR008800.

Zhao, M., and S. W. Running (2010), Drought-induced reduction in global terrestrial net primary production from 2000 through 2009, *Science*, *329*, 940–943, doi:10.1126/science.1192666.

Zheng, G., J. M. Chen, Q. Tian, W. M. Ju, and X. Q. Xia (2007), Combining remote sensing imagery and forest age inventory for biomass mapping, *J. Environ. Manage.*, *85*, 616–623, doi:10.1016/j.jenvman.2006.07.015.

Zhu, G. L., et al. (2010), Forest canopy leaf area index in Maoershan Mountain: Ground measurement and remote sensing retrieval [in Chinese], *Chin. J. Appl. Ecol.*, *21*, 2117–2124.